Title

Curvature of Radial Electric Field Aggravates Edge Magnetohydrodynamics Mode in Toroidally Confined Plasmas

Journal

Physical Review Letters, 125(25)

ISSN

0031-9007

Authors

Zhang, Y
Guo, ZB
Diamond, PH

Publication Date

2020-12-18

DOI

10.1103/physrevlett.125.255003

Peer reviewed

Curvature of Radial Electric Field Aggravates Edge Magnetohydrodynamics Mode in Toroidally Confined Plasmas

Y. Zhang,[1] Z. B. Guo,[1,*] and P. H. Diamond[2]

[1]State Key Laboratory of Nuclear Physics and Technology, Fusion Simulation Center, School of Physics, Peking University, Beijing 100871, China

[2]University of California San Diego, La Jolla, California 92093, USA

(Received 20 July 2020; revised 24 November 2020; accepted 30 November 2020; published 18 December 2020)

We show that the radial electric field (E_r) plays a dual role in edge magnetohydrodynamics (MHD) activity. While E_r shear (first spatial derivative of E_r) dephases radial velocity and displacement, and so is stabilizing, a new finding here is that E_r curvature (second spatial derivative of E_r) tends to synchronize the radial velocity and displacement, and so destabilizes MHD. As a highlighted result, we analytically demonstrate that E_r curvature can destabilize an otherwise stable kink mode, and so form a joint vortex-kink mode. The synergetic effects of E_r shear and E_r curvature in edge MHD extend the familiar $E \times B$ shearing paradigm. This theory thus explains the experimental findings that a deeper $E \times B$ well may aggravate edge MHD, and so trigger the formation of the edge harmonic oscillation. A simple criterion linking E_r structure and the edge MHD activity is derived.

DOI: 10.1103/PhysRevLett.125.255003

Boundary layers are narrow regions, where various physical quantities transition and change sharply. They are ubiquitous features of bounded systems and are essential players in important physical issues, such as laminar-to-turbulence transition, turbulent drag phenomena, etc. [1]. Linear and nonlinear stability of the boundary layers are key issues in many areas of continuum physics.

The edge (also known as pedestal region) of a toroidally confined plasma is a quintessential example of boundary layers. Its formation and stability are crucial to high-confinement mode operation of fusion devices, e.g., the International Thermonuclear Experimental Reactor. However, a narrow edge can support either hazardous low-frequency magnetohydrodynamics (MHD) instabilities [2], i.e., edge localized mode or benign high-frequency edge harmonic oscillations (EHOs) [3–5]. It is a challenging problem to address the physical mechanism of which type of edge MHD phenomena will be excited in such a narrow layer. Peeling-ballooning (PB) modes are the most studied ideal edge MHD instabilities. These are driven by the free energy stored in the current density (j_0) and the plasma pressure (P_0) profiles [6,7]. The radial electric field is conventionally thought to impact the PB mode through $E \times B$ flow shear (i.e., E_r shear). However, this limited view is inadequate because a strong $E \times B$ flow in the edge region inevitably produces another free energy source—the vorticity profile (ω_0), which may drive edge instability through its gradient (i.e., E_r curvature). Therefore, to characterize the edge MHD activity in the presence of $E \times B$ flow, *both* E_r shear and E_r curvature must be considered.

In this Letter, we report a new approach to study edge MHD modes by considering the phase coupling of vortex waves produced by different sources. The vortex-wave interaction theory was proposed to interpret the underlying physical mechanism of shear flow instabilities [8]. For example, with this theory, the well-known Kelvin-Helmholtz instability is shown to be induced by phase locking of two neutrally stable interfacial vortex waves [9–11]. In the edge region of toroidal plasmas, it is the interaction of three types of vortex waves (produced by j_0, P_0, and ω_0 gradients) that determines the excitation of the edge MHD mode. In an idealized setup of mean current density and vorticity profiles, we show that the (neutrally stable) vortex wave produced by the E_r curvature is "locked" to that by the j_0 gradient, so the phase of the radial velocity is pinned to that of the radial displacement, and a joint vortex-kink mode is excited. For the mode driven jointly by ω_0, j_0, and P_0 gradients, we also carry out numerical simulations in the framework of toroidal reduced MHD. Our results indicate that the average ratio ($\mathcal{R}$) of E_r curvature to E_r shear in the edge region determines how the structure of the E_r profile impacts edge MHD instability. By moving the trough of the E_r well outward, a larger $\mathcal{R}$ will be induced and the low-n MHD mode (e.g., EHO) tends to be excited. While moving the trough inward, $\mathcal{R}$ will become smaller, and the edge tends to be stabilized.

In order to illustrate the relation between phase coupling and instability, we consider the evolution of a radial displacement $\tilde{\xi}_r = \mathrm{Re}(|\hat{\xi}_r(r,t)|e^{i\vartheta_{\xi_r}(r,t)}e^{im\theta - ik_z z})$, which is subjected to a radial velocity disturbance $\tilde{v}_r = \mathrm{Re}(|\hat{v}_r(r,t)|e^{i\vartheta_{v_r}(r,t)}e^{im\theta - ik_z z})$. In cylindrical coordinates (r, θ, z), m, and k_z are the wave numbers in θ and z

directions, and ϑ_{ξ_r} and ϑ_{v_r} are the phases of $\hat{\xi}_r$ and $\hat{v}_r$, respectively. The evolutions of $|\hat{\xi}_r|$ and ϑ_{ξ_r} follow as

$$\frac{\partial}{\partial t}|\hat{\xi}_r| = |\hat{v}_r|\cos(\vartheta_{v_r} - \vartheta_{\xi_r}), \tag{1}$$

$$\frac{\partial}{\partial t}\vartheta_{\xi_r} = -k_\theta V_{E\times B} + \frac{|\hat{v}_r|}{|\hat{\xi}_r|}\sin(\vartheta_{v_r} - \vartheta_{\xi_r}), \tag{2}$$

where $k_\theta = m/r$, and $V_{E\times B}$ is the mean $E\times B$ velocity induced by the radial electric field. Equations (1) and (2) reflect the formation of an instability. They are reduced to an eigenmode description after the transformations, $\partial_t|\hat{\xi}_r| = \gamma_\xi|\hat{\xi}_r|$ and $\partial_t\vartheta_{\xi_r} = -\omega_\xi$, with γ_ξ as the growth rate and ω_ξ as the eigenfrequency. Equation (1) shows that the phase difference between the radial velocity and displacement determines whether or not $|\hat{\xi}_r|$ will grow. From Eq. (2), one can see that the $E\times B$ flow shear tends to dephase the displacements at different radial locations, so that it may induce phase slips and saturate the affected mode. This effect has been discussed in Ref. [12]. For the $E\times B$ type velocity disturbance, one has $\hat{v}_r = -\nabla_\theta\hat{\phi}\times\hat{z} = -im\hat{\phi}/r$ and $\vartheta_{v_r} = -\pi/2 + \vartheta_\phi$ (ϑ_ϕ is the phase of $\hat{\phi}$). The normalized electrostatic potential $\hat{\phi}$ is related to the vorticity perturbation $\hat{\omega}$ via $\partial_r(r\partial_r\hat{\phi})/r - m^2\hat{\phi}/r^2 = \hat{\omega}$. $\hat{\phi}$ can be solved for as

$$\hat{\phi}(r,t) = \int_0^{+\infty} G(r,r')\hat{\omega}(r',t)dr', \tag{3}$$

where the Green's function is $G(r,r') = -1/(2m)[(r/r')^m H(r'-r) + (r'/r)^m H(r-r')]$ with $H(x)$ as the Hankel function. The poloidal mode number m reflects the nonlocality of the $\hat{\phi}-\hat{\omega}$ coupling. A smaller m means a longer range of coupling. With $\hat{\xi}_r = \int_0^t \hat{v}_r(t')dt'$, the cross phase $(\vartheta_{v_r} - \vartheta_{\xi_r})$ is thus uniquely determined by the spatial distribution of the vorticity field. The instability problem is then translated into a general problem of how the vorticity disturbances produced by different free energy sources interact with each other and influence the growth of the displacement.

Vortex-Kink mode.—For analytical tractability, we start with the joint mode driven by the current density gradient and the vorticity gradient (i.e., the E_r curvature) in the framework of cylindrical reduced MHD [13,14]. Its linearized form is cast as

$$\left(\frac{\partial}{\partial t} + V_{E\times B}\nabla\right)\tilde{\omega} = -\tilde{v}_r\omega_0' + \tilde{B}_r j_0' + B_0\nabla\tilde{j}, \tag{4}$$

$$\left(\frac{\partial}{\partial t} + V_{E\times B}\nabla\right)\tilde{\psi} = -\tilde{v}_r\psi_0' + B_{0,z}\frac{\partial\tilde{\phi}}{\partial z}, \tag{5}$$

where we have set the mean density $\rho_0 = 1$ and the speed of light $c = 1$. The total vorticity $\omega = \omega_0 + \tilde{\omega} = \nabla_\perp^2\phi_0 + \nabla_\perp^2\tilde{\phi}$ where $\tilde{\cdot}$ (the subscript "0") denotes the perturbed (mean) quantities, and $'$ denotes the radial gradient. ψ is the magnetic vector potential in z direction and the total current density $j = j_0 + \tilde{j} = \nabla_\perp^2\psi_0/(4\pi) + \nabla_\perp^2\tilde{\psi}/(4\pi)$. The first term on the rhs of Eq. (4) is the kinematic vorticity source associated with the mean vorticity gradient [10], the second term is the vorticity source produced by the electromagnetic torque, associated with the mean current density gradient, and the third term is the Alfvnic effect of the mean magnetic field. We employ idealized steplike profiles to mimic the rapid variations of ω_0 and j_0 in the edge region [Fig. 1(a)]. Then, Eqs. (4) and (5) are simple enough to permit an analytical eigenmode solution. Using the transformations $\tilde{\phi}(\tilde{\psi}) = \hat{\phi}(\hat{\psi})e^{-i(\Omega+k_\theta V_{E\times B})t+im\theta-ik_z z}$ and eliminating $\hat{\psi}$ in Eq. (4) yields

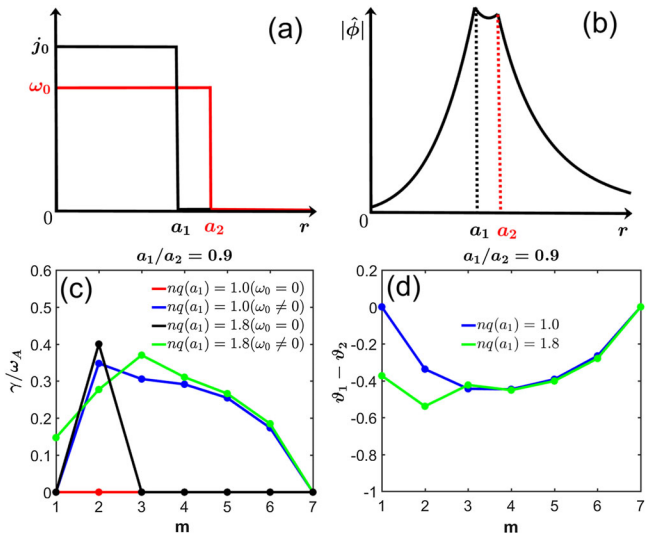

FIG. 1. (a) Current density (j_0) and vorticity (ω_0) distributions used in the theoretical model. (b) The eigenfunction's amplitude of the joint mode, where $c_0 = 1.0328$, $c_1 = 0.6791$, $c_2 = 0.599$, $c_3 = 1.0$, $a_1/a_2 = 0.9$, and $m = 5$. (c) The growth rate $\gamma = \Im(\Omega)$ of vortex-kink mode with $a_1/a_2 = 0.9$, and (d) the cross phase of the two interfacial vortex waves at $r = a_1$ and $r = a_2$. Here the growth rate is normalized to the Alfvén frequency at a_1 (i.e., $\omega_A = B_{0,\theta}/\sqrt{4\pi\rho_0 a_1^2}$), and the mean vorticity is set as $\omega_0 = 1.2\omega_A$. The two vortex waves are decoupled when $m > 7$, i.e., $k_\theta|a_2 - a_1| > 0.6223$.

$$\Omega\nabla_\perp^2\hat{\phi} = -k_\theta\omega_0'\hat{\phi} + \frac{k_\theta k_\parallel B_0}{\Omega}j_0'\hat{\phi} + \frac{k_\parallel^2 B_0^2}{4\pi\Omega}\nabla_\perp^2\hat{\phi}, \tag{6}$$

where $k_z = n/R_0$ (R_0, the major radius; n, mode number in z), and $k_\parallel B_0 = -B_{0,\theta}(m - nq)/r$ with $q = (rB_{0,z})/(R_0 B_{0,\theta})$ as the safety factor. Neglecting the Alfvnic effect ($O(k_\parallel^2)$), Eq. (6) is reduced to a type of Taylor-Goldstein equation [15,16]. Hence, we expect that the resonant interaction between the vorticity and the

current density layers would be essential to joint instability. $\hat{\phi}$'s eigenfunction has the following form [Fig. 1(b)]:

$$\hat{\phi}(r) = \begin{cases} c_0\left(\frac{r}{a_1}\right)^m & \text{at } r < a_1 \\ c_1\left(\frac{a_1}{r}\right)^m + c_2\left(\frac{r}{a_2}\right)^m & \text{at } a_1 \le r \le a_2 \\ c_3\left(\frac{a_2}{r}\right)^m & \text{at } r > a_2 \end{cases} \quad (7)$$

The coefficients c_i $(i = 0, 1, 2, 3)$ are constrained by the matching conditions

$$c_0 = c_1 + c_2\left(\frac{a_1}{a_2}\right)^m, \quad (8)$$

$$c_3 = c_2 + c_1\left(\frac{a_1}{a_2}\right)^m, \quad (9)$$

$$\Omega\Delta_1 = \frac{k_{||}^2 B_0^2}{4\pi\Omega}\Delta_1 - \frac{B_\theta}{2\pi a_1}\frac{k_\theta k_{||} B_0}{\Omega}\hat{\phi}(a_1), \quad (10)$$

$$\Omega\Delta_2 = \frac{k_{||}^2 B_0^2}{4\pi\Omega}\Delta_2 + k_\theta\omega_0\hat{\phi}(a_2), \quad (11)$$

where $\Delta_1 = m[-c_1 + c_2(a_1/a_2)^m - c_0]/a_1$, $\Delta_2 = m[-c_3 + c_1(a_1/a_2)^m - c_2]/a_2$. Equations (8) and (9) follow from the continuity of $\hat{\phi}(r)$ at $r = a_1$ and $r = a_2$, and Eqs. (10) and (11) are from the integral of Eq. (6) over the narrow intervals at $r = a_1$ and $r = a_2$. The dispersion relation is obtained by reorganizing Eqs. (8)–(11) into a matrix representation $\boldsymbol{Mc} = 0$ and setting the determinant $|\boldsymbol{M}| = 0$, where $\boldsymbol{c} = (c_0, c_1, c_2, c_3)^T$. The eigenmode growth rate is given by $\gamma = \Im(\Omega)$.

It is well known that, in the absence of ω_0, for a step j_0 profile, the kink mode is neutrally stable if nq is an integer [red in Fig. 1(c)] [17,18]. It is also straightforward to check that, for $j_0 = 0$, the kinematic vortex wave is also neutrally stable. Therefore, by choosing nq as an integer ($nq = 1$ here), we have a setup of two neutrally stable interfacial vortex waves produced by j_0' and ω_0' at a_1 and a_2, respectively. Here we choose $a_1/a_2 < 1$. For $a_1/a_2 > 1$, the results are similar. First, we give an intuitive demonstration of the relation between the phase coupling of vortex waves and the joint mode instability. As sketched in Fig. 2, to form a joint instability, the two neutrally stable interfacial vortex waves should be phase locked (resonant interaction) [8], with their phases ϑ_1 and ϑ_2 given by $c_0 = |c_0|e^{i\vartheta_1}$ and $c_3 = |c_3|e^{i\vartheta_2}$, respectively. Assuming $k_\theta|a_2 - a_1| \ll 1$, for $\vartheta_1 = \vartheta_2$, the two vortex waves are in phase and they form a neutrally stable joint mode. If $0 < \vartheta_1 - \vartheta_2 < \pi$, the two waves tend to limit each other; i.e., the joint mode is a damped one. The joint mode is destabilized if $-\pi < \vartheta_1 - \vartheta_2 < 0$, because the two vortex waves strengthen each other. This is confirmed by Fig. 1(d) (blue), where $-\pi < \vartheta_1 - \vartheta_2 < 0$ for the unstable joint mode and $\vartheta_1 - \vartheta_2 = 0$ for the neutrally stable one. It is also consistent with the eigenmode analysis, showing the

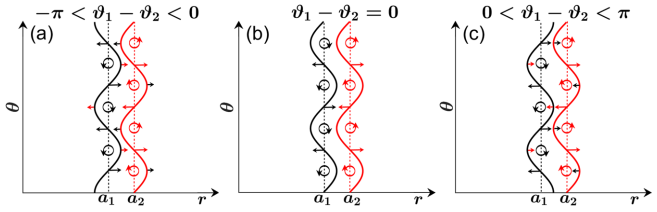

FIG. 2. A schematic illustration of the relationship between vortex-wave interaction and joint mode instability. The red horizontal arrows at the peaks and troughs of the black wave field represent the displacement induced by the red wave field. The black arrows at the red wave field are induced by the black wave field. The two vortex waves are phase locked, and depending on the phase difference $(\vartheta_1 - \vartheta_2)$, the joint mode could be (a) unstable, (b) neutrally stable, (c) stable.

kink mode could be destabilized if $\omega_0' \neq 0$ [blue, Fig. 1(c)]. A twist is that, if initially the kink mode is unstable [black, Fig. 1(c)], the growth rate of the joint mode may be smaller than that of the pure kink mode [green, $m = 2$ in Fig. 1(c)]. To understand this, we decompose the displacement near $r = a_1$ into two pieces, $\tilde{\xi} = \tilde{\xi}_1 + \tilde{\xi}_2$ with $\tilde{\xi}_1(\tilde{\xi}_2)$ produced by the vortex disturbance at $a_1(a_2)$. The growth rate of the joint mode can be expressed as $\gamma_{\text{eff}} = (\gamma_1\tilde{\xi}_1 + \gamma_2\tilde{\xi}_2)/(\tilde{\xi}_1 + \tilde{\xi}_2) = \gamma_1 + \tilde{\xi}_2(\gamma_2 - \gamma_1)/(\tilde{\xi}_1 + \tilde{\xi}_2) = \gamma_2 + \tilde{\xi}_1(\gamma_1 - \gamma_2)/(\tilde{\xi}_1 + \tilde{\xi}_2)$, where $\gamma_{1(2)}\tilde{\xi}_{1(2)} = \partial_t\tilde{\xi}_{1(2)}$ and γ_1 is the growth rate of the pure kink mode. For $-\pi < \vartheta_1 - \vartheta_2 < 0$, $\tilde{\xi}_1$ and $\tilde{\xi}_2$ have the same sign and hence $\min(\gamma_1, \gamma_2 < \gamma_{\text{eff}} < \max(\gamma_1, \gamma_2)$. Through the analytical solution for the piecewise continuous mean profiles, we have an understanding of the essential physics of the joint mode formation.

For more realistic j_0 and ω_0 profiles, an analytical eigenmode solution is generally forbidden. The vortex-wave interaction theory has the advantage of providing a physical understanding of how an instability forms. We carry out direct simulations of Eqs. (4) and (5) with the j_0 and ω_0 profiles given by Fig. 3(a). As our focus is the effect of the E_r profile (E_r shear and E_r curvature), we keep the j_0 profile fixed and set the kink mode driven by

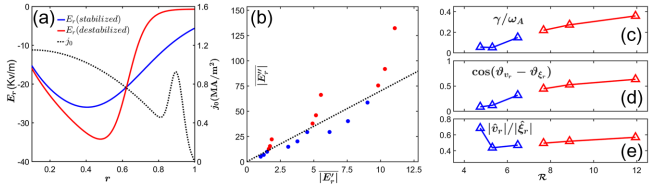

FIG. 3. (a) Mean current density (dashed line) and E_r profiles (solid lines) in SI units. (b) Impact of E_r profile on a unstable kink mode. Both $|\overline{E_r'}|$ and $|\overline{E_r''}|$ are in dimensionless form. Red (blue) marker means the growth rate of the joint mode is larger (smaller) than that of the pure kink. (c) Growth rate of the vortex-kink mode. (d) The spatially averaged cosine of cross phase between $\hat{v}_r$ and $\hat{\xi}_r$. (e) The spatially averaged amplitude ratio $|\hat{v}_r|/|\hat{\xi}_r|$. The toroidal mode number is $n = 3$.

j_0' unstable in our simulations. By implementing a series of different E_r profiles, it is shown in Fig. 3(b) that a larger $\overline{|E_r''|}$ tends to further destabilize the pure kink mode, while a larger $\overline{|E_r'|}$ tends to stabilize the kink mode. To measure the relative effect of E_r curvature verse E_r shear, we define a dimensionless parameter $\mathcal{R} \equiv \overline{|E_r''|}/\overline{|E_r'|}$ (r is normalized by the small radius), where $\overline{|E_r''|} = \int_0^1 |E_r''|dr$ and $\overline{|E_r'|} = \int_0^1 |E_r'|dr$. In contrast to the piecewise profiles, the vortex disturbances produced by the current density and vorticity fields in Fig. 3(a) are not localized to an interface. Then, a direct way to see the influence of vortex-wave interaction on the mode growth is studying the phase difference, $\vartheta_{v_r} - \vartheta_{\xi_r}$ [Eqs. (1) and (2)]. As shown in Fig. 3(d), $\hat{v}_r$ and $\hat{\xi}_r$ become more synchronized by increasing $\mathcal{R}$ and are dephased by decreasing $\mathcal{R}$. According to Eq. (1), the formal expression of the growth rate is $\gamma = \partial_t \ln|\hat{\xi}_r| = (|\hat{v}_r|/|\hat{\xi}_r|)\cos(\vartheta_{v_r} - \vartheta_{\xi_r})$. Overall, $\mathcal{R}$ impacts the growth rate mainly through modulating the cross phase. In summary, $\mathcal{R}$ is the proper quantity to quantify the E_r profile effect, in contrast to the familiar E_r shear or shearing paradigm [19].

Vortex-kink-ballooning mode.—There is accumulating experimental and simulation evidence indicating that a deeper E_r well may facilitate the excitation of a low-n edge MHD mode, e.g., the EHO [3,19–21], other than having a stabilizing effect. These facts point to a reconsideration of the E_r and MHD interaction in the edge region, i.e., incorporating the driving effect by E_r curvature. The simplest framework within which to study the joint mode driven by j_0', P_0', and ω_0' in the edge region is the toroidal reduced MHD equations [22,23], i.e., replacing Eq. (4) by

$$\left(\frac{\partial}{\partial t} + V_{E\times B}\nabla\right)\tilde{\varpi} = -\tilde{v}_r\omega_0' + \tilde{B}_r j_0' + B_0\nabla\tilde{j} + b_0\kappa_0 \times \nabla_\perp\tilde{p}, \tag{12}$$

and adding the pressure perturbation $\tilde{p}$'s evolution equation

$$\left(\frac{\partial}{\partial t} + V_{E\times B}\nabla\right)\tilde{p} = -\tilde{v}_r P_0', \tag{13}$$

where $\tilde{\varpi} = \tilde{\omega} + \nabla_\perp^2\tilde{p}/(en_0)$, $b_0 = \boldsymbol{B}_0/|B_0|$ and $\kappa_0 = b_0\nabla b_0$ is the curvature of the mean magnetic field line. We carry out our simulation by using the three fields BOUT++ code [23]. As in the vortex-kink simulation, we fix the current density and pressure profiles and vary the E_r profile to study how E_r influences the excitation of the joint mode. Both the amplitude and the shape of the E_r adopted here [Fig. 4(b)] are similar to those in experiments [24]. A direct way to uncover the features of the E_r structure is to decompose it into a symmetric piece (E_S) and an anti-symmetric piece (E_{AS}), i.e., $E_r = E_S + E_{AS}$ [Fig. 4(b)]. E_S is fixed and E_{AS} is set by $E_{AS} = \sigma B_\theta R_0(D_0\{1 - \tanh[D_s(r - r_0)]\} + C)$ with $\sigma = \pm 1$, R_0 as the major radius, $D_0 = 45$ krad/s, $C = 3$ krad/s, and $r_0 = 0.855$

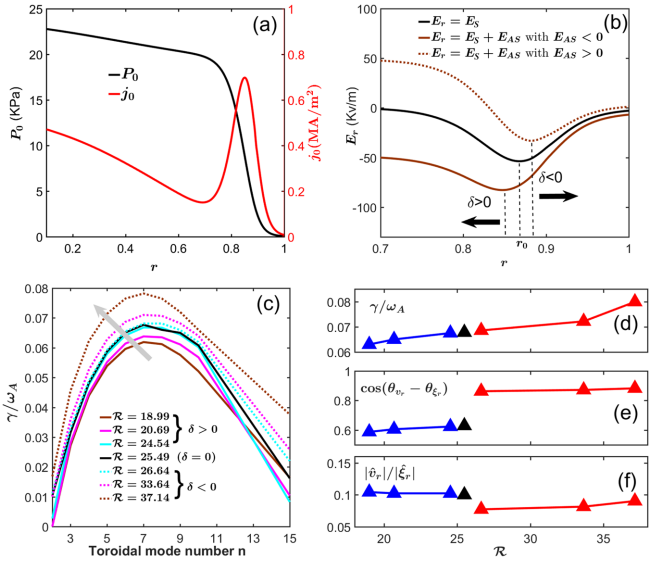

FIG. 4. (a) The equilibrium pressure (black line) and current density (red line) profiles. (b) Three typical E_r profiles. (c) The linear growth rate spectrum for different $\mathcal{R}$. (d) The growth rate of the $n = 7$ mode. (e) The spatially averaged cosine of cross phase $(\vartheta_{v_r} - \vartheta_{\xi_r})$. (f) The spatially averaged amplitude ratio $|\hat{v}_r|/|\hat{\xi}_r|$.

(the trough of E_S) [25]. Different E_r profiles are obtained by changing D_s. δ is the shift of the E_r well trough relative to the symmetric one. Physically, E_r is determined by various kinetic processes such as ion pressure gradient, ion rotation, ion orbit loss, etc. [26], which are beyond the MHD model employed in the current Letter. Figure 4(c) is the linear growth rate spectrum of the joint mode for a series of E_r profiles. It clearly shows that, by increasing $\mathcal{R}$, the joint instability is enhanced [dashed, Fig. 4(c)]. It is weakened [solid, Fig. 4(c)] by reducing $\mathcal{R}$. Interestingly, E_r curvature has a larger destabilizing effect on the relatively low-n mode, because there the vortex coupling is stronger. The trend of the cross phase with $\mathcal{R}$ is similar to that of the vortex-kink scenario [Fig. 3(d)].

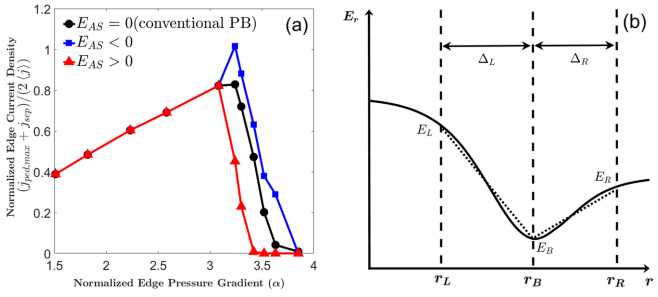

FIG. 5. (a) Marginal boundaries of the joint mode and the conventional PB mode. The red line corresponds to increase of $\mathcal{R}$ and the blue line to decrease of $\mathcal{R}$ with $D_0 = 10$ krad/s and $D_s = 35$. (b) A schematic sketch of the E_r well. $[r_L, r_R]$ is chosen as the edge region.

It is well documented that the edge-localized mode (ELM)-free H mode sits *just* below the boundary of the conventional PB mode [27]. An outstanding question is how the EHO (here proposed as the joint mode) is excited. A proper way to address this issue is choosing different E_{AS} and compare the marginal boundary of the joint mode with that of the PB mode. The results are shown in Fig. 5(a). It reveals that the enhancement of $\mathcal{R}$ ($E_{\mathrm{AS}} > 0$) significantly moves the boundary of the joint mode to the stable regime of the PB mode for large α, which corresponds to the H mode. As a consequence, the joint mode is excited before α encounters the conventional PB boundary, beyond which the ELM is triggered. In other words, the E_r curvature can facilitate the transition of ELMy H mode to ELM-free H mode. To link the proceeding theoretical analysis to experiments, assuming a U shape E_r well [Fig. 5(b)], it is straightforward to show that

$$\mathcal{R} \simeq \frac{1}{\Delta_L}\left[1 - \frac{E_R - E_B}{E_R + E_L - 2E_B}\frac{\delta}{\Delta_L}\right], \tag{14}$$

where $E_{L(R)}$ is the electric field at the left (right) margin $r_{L(R)}$, E_B is the trough of the E_r well and $\delta = \Delta_R - \Delta_L$. Since E_L, $E_R > E_B$, if $\delta < 0$, $\mathcal{R}$ will be enhanced and the edge mode is destabilized [dashed lines, Fig. 4(c)]. If $\delta > 0$, the edge mode is weakened because $\mathcal{R}$ is reduced [solid lines, Fig. 4(c)].

In conclusion, these results significantly extend and alter the widely invoked ideal peeling-ballooning model of edge MHD. It also opens new territory for studying couplings of microscopic modes.

We would like to acknowledge X. Q. Xu, Z. Y. Li, D. Hu, Z. J. Mao, and Y. Lang for useful discussions. We are also grateful to W. M. Chen, B. Gui, G. Q. Dong, and B. Dudson for technical help. We acknowledge fruitful interactions with participants in the Festival de Thorie, Aix-en-Provence (2019). This project was supported by the National MCF Energy R&D Program (2018YFE0311400) and by the U.S. Department of Energy, Office of Science, Office of Fusion Energy Sciences under Award No. DE-FG02-04ER54738. The numerical simulations were supported by the High-Performance Computing Platform of Peking University.

*Corresponding author.
zbguo@pku.edu.cn

[1] H. Schlichting and K. Gersten, *Boundary-Layer Theory* (Springer, New York, 2016).
[2] A. W. Leonard, Phys. Plasmas **21**, 090501 (2014).
[3] K. H. Burrell, M. E. Austin, D. P. Brennan *et al.*, Phys. Plasmas **8**, 2153 (2001).
[4] A. A. Garofalo, W. A. Solomon, and J. K. Park, Nucl. Fusion **51**, 083018 (2011).
[5] T. M. Wilks, A. M. Garofalo, P. H. Diamond, Z. Guo, J. W. Hughes, K. H. Burrell, and X. Chen, Nucl. Fusion **58**, 112002 (2018).
[6] J. W. Connor, R. J. Hastie, H. R. Wilson, and R. L. Miller, Phys. Plasmas **5**, 2687 (1998).
[7] P. B. Snyder, H. R. Wilson, J. R. Ferron, L. L. Lao, A. W. Leonard, T. H. Osborne, A. D. Turnbull, D. Mossessian, M. Murakami, and X. Q. Xu, Phys. Plasmas **9**, 2037 (2002).
[8] J. R. Carpenter, E. W. Tedford, E. Heifetz, and G. A. Lawrence, Appl. Mech. Rev. **64**, 061001 (2013).
[9] J. W. S. Rayleigh, Proc. Math. Soc. **12**, 57 (1880).
[10] J. Holmboe, Geophys. Publ. **24**, 67113 (1962).
[11] A. Guha and G. A. Lawrence, J. Fluid Mech. **755**, 336 (2013).
[12] Z. B. Guo and P. H. Diamond, Phys. Rev. Lett. **114**, 145002 (2015).
[13] B. B. Kadomtsev and O. P. Pogutse, *Reviews of Plasma Physics* (Springer, New York, 1970), p. 249.
[14] H. R. Strauss, Phys. Fluids **19**, 134 (1976).
[15] G. I. Taylor, Proc. R. Soc. A **132**, 499 (1931).
[16] S. Goldstein, Proc. R. Soc. A **132**, 524 (1931).
[17] B. B. Kadomtsev, *Tokamak Plasma: A Complex Physical System* (Institute of Physics Publ., 1992).
[18] J. A. Wesson, Nucl. Fusion **18**, 87 (1978).
[19] J. G. Chen, X. Q. Xu, C. H. Ma, P. W. Xi, D. F. Kong, and Y. A. Lei, Phys. Plasmas **24**, 050704 (2017).
[20] A. M. Garofalo, K. H. Burrell, D. Eldon *et al.*, Phys. Plasmas **22**, 056116 (2015).
[21] F. Liu, G. T. A. Huijsmans, A. Loarte, A. M. Garofalo, W. M. Solomon, P. B. Snyder, M. Hoelzl, and L. Zeng, Nucl. Fusion **55**, 113002 (2015).
[22] R. D. Hazeltine and J. D. Meiss, *Plasma Confinement* (Courier Corporation, Chelmsford, MA, 2003).
[23] X. Q. Xu, B. Dudson, P. B. Snyder, M. V. Umansky, and H. Wilson, Phys. Rev. Lett. **105**, 175005 (2010).
[24] K. H. Burrell, M. E. Austin, D. P. Brennan *et al.*, Plasma Phys. Controlled Fusion **44**, A253 (2002).
[25] Y. Zhang, Z. B. Guo, X. Q. Xu, and J. G. Chen, Phys. Plasmas **26**, 052508 (2019).
[26] C. S. Chang, S. Ku, and H. Weitzner, Phys. Plasmas **11**, 2649 (2004).
[27] P. B. Snyder *et al.*, Nucl. Fusion **47**, 961 (2007).